

Many-body multipole indices revealed by the real-space dynamical mean-field theory

Guoao Yang,¹ Jianhui Zhou,^{2,*} and Tao Qin^{1,†}

¹*School of Physics and Optoelectronics Engineering,
Anhui University, Hefei, Anhui Province 230601, P.R. China*

²*Anhui Key Laboratory of Low-energy Quantum Materials and Devices,
High Magnetic Field Laboratory, HFIPS, Chinese Academy of Sciences, Hefei, Anhui 230031, China*

The multipole moments are fundamental properties of insulators, and have attracted lots of attention with emerging of the higher-order topological insulators. A couple of ways, including generalization of the formula for the polarization and the Wilson loop, have been proposed to calculate it in real materials. However, a practical method to explore it in correlated insulators is still lacking. Here, we proposed a systematic way, which combines the general Green's function formula for multipoles with the real-space dynamical mean-field theory, to calculate the multipole moments in correlated materials. Our demonstrating calculations are consistent with symmetry analysis, and the calculations of the spectral functions further confirm our results. This method opens the new avenue to study the topological phase transitions in correlated multipole insulators and other crucial physical quantities closely related to multipole moments.

I. INTRODUCTION

The polarization is a fundamental property of insulators, and it has been under intensive study for decades [1–7]. It is a ground-breaking progress to realize that the change of polarization is closely related to the integral of the Berry curvature in the parameter space [1, 2]. The emergence of topological insulators offers a new platform for the study of polarization, which works as a topological index for the topological phase transition. However, for a long time, a systematic method to reveal the polarization in a correlated insulator remains elusive, even if there are detailed discussion on this formalism [4, 8]. In Resta's pioneering work [9], a formula for the polarization is proposed, and affords the possibility of exploring the polarization in the interacting case. Furthermore, with the concept of localization length [10], its connection with Kohn's theory of insulating state [11] has been established. To explore the properties of multipole moments, which offers a distinctive point of view to uncover the nontrivial topological physics, is fundamentally important.

The topics on the polarization and its multipole generalization have become more active with the generalized concept of higher-order topological insulator. The higher-order topological phase, which is a key playground for multipole indices, is characterized by the quantized multipole indices, pioneered by Benalcazar *et al.* [12]. This novel concept has been identified in different non-crystalline lattices without periodicity [13, 14]. The generalization of Resta's formula to the multipole case has opened the avenue to study the multipole [15], which can serve as an index to classify the higher-order topological insulators. Even though a couple of issues have been pointed out in this generalization [16], detailed calculations have been done for non-interacting models [17], and

its effectiveness has been verified. Its relationship with the Wilson-loop formulation [12, 18] has been elaborated. Furthermore, several ways have been tried out to study multipole indices of correlated insulator. In Ref. [19], the polarization of the Hubbard model is explored with the dynamical mean-field theory (DMFT) [20]. However, it is hard to apply it to the multipole moments. In Ref. [21], correlation effects in quadrupole insulators are studied with the quantum Monte Carlo simulations and topological Hamiltonians. In Ref. [22] a many-body invariant is extracted from Resta's operator for the polarization with methods of exact diagonalization and infinite density matrix renormalization group. Clearly, these are indirect ways to calculate the multipole indices in correlated systems.

However, a practical procedure for directly calculating the many-body multipole index of correlated insulators is still lacking. Here, we propose a Green's function formalism in the real space for the multipole indices, which can be perfectly fitted into the scheme of the real-space dynamical mean-field theory (R-DMFT) [23–25]. We have carried out calculations of multipole indices of the correlated Benalcazar-Bernevig-Hughes (BBH) model with different spatial symmetries. The results are consistent with the symmetry analysis, and shed light on the exploration of multipole indices of the correlated insulator. Furthermore, we would like to point out that our formalism can be adopted to study the higher-order topological phase in crystalline systems with quenched disorder and in non-crystalline systems, and that it also affords a way to compute the localization length of the electron [10], the polarization fluctuation [26], and the quantum geometric tensor [27] in the correlated lattices.

The rest of the manuscript has been organized as follows. In Sec. II, we show our derivation details for the general formula of the multipoles, explain our protocol on how to combine them with the R-DMFT, and point out its further generalization. In Sec. III, we show our demonstrating calculation results for the correlated BBH model with different spatial symmetries. A summary and

* jhzhou@hmf.ac.cn

† taoqin@ahu.edu.cn

outlook is presented in Sec. IV.

II. MANY-BODY MULTIPOLE INDICES IN GREEN'S FUNCTION FORMALISM

We propose a Green's function formalism for the electrical polarization for a crystal, which is ready to be studied in a correlated system,

$$P_x = \frac{1}{2\pi\mathcal{S}} \text{Im} \left[\text{Tr} \ln \left(\tilde{G}_x + I \right) \right] - P_{bg}. \quad (1)$$

This is the central result in this work. Here $\tilde{G}_x = \alpha_x G$. $\alpha_x = \text{diag}\{e^{\frac{2\pi i x_1}{L_x}} - 1, \dots, e^{\frac{2\pi i x_N}{L_x}} - 1\}$, and G_x is a matrix of Green's function with the i, j -th element as $\langle c_i^\dagger c_j \rangle = \frac{1}{\beta} \sum_n G_{ij}(\omega_n)$, where $\omega_n = \frac{(2n+1)\pi}{\beta}$ is the Matsubara frequency, and c_i^\dagger (c_j) is the creation (annihilation) operator on the lattice site i (j) in a supercell with sizes as L_x , $L_x L_y$, and $L_x L_y L_z$ for one, two and three-dimensional cases, respectively. I is the identity matrix. \mathcal{S} is dimension-dependent as $\mathcal{S} = 1, L_y, L_y L_z$ for different dimensions, which is the area perpendicular to the x direction. $P_{bg} = \frac{n_f}{\mathcal{S}} \sum_i \frac{x_i}{L_x}$ is the contribution from the background charge, with n_f the local density of electrical states. It can be combined with fixed boundary condition, periodic boundary condition and a hybrid boundary condition. The generalization to include the spin flavor is straightforward.

We outline the crucial derivation steps for Eq. (1). Starting from the formula [9, 15], $P_x = \frac{1}{2\pi\mathcal{S}} \text{Im} \left[\ln \langle \hat{U}_x \rangle \right] - P_{bg}$, where $\langle \hat{U}_x \rangle = \langle GS | \hat{U}_x | GS \rangle = \langle GS | e^{2\pi i \sum_l \frac{x_l}{L_x} \hat{n}_l} | GS \rangle$, we have,

$$\langle \hat{U}_x \rangle = \langle GS | e^{2\pi i \frac{x_1}{L_x} \hat{n}_1} e^{2\pi i \frac{x_2}{L_x} \hat{n}_2} \dots e^{2\pi i \frac{x_N}{L_x} \hat{n}_N} | GS \rangle. \quad (2)$$

For the electron, we note the nilpotency property of the electron number operator $\hat{n}_l^2 = \hat{n}_l$, which is a key observation here, and it follows that $e^{2\pi i \frac{x_l}{L_x} \hat{n}_l} = \sum_{m=0}^{\infty} \frac{1}{m!} \left(2\pi i \frac{x_l}{L_x} \hat{n}_l \right)^m = 1 + \alpha_l \hat{n}_l$ with $\alpha_l = e^{\frac{2\pi i x_l}{L_x}} - 1$. Therefore, we come to

$$\begin{aligned} \langle \hat{U}_x \rangle &= \langle GS | \prod_{l=1}^N (1 + \alpha_l \hat{n}_l) | GS \rangle, \\ &= 1 + \sum_{l=1}^N \alpha_l \langle \hat{n}_l \rangle + \sum_{1 \leq i < j \leq N} \alpha_i \alpha_j \langle \hat{n}_i \hat{n}_j \rangle + \dots, \end{aligned} \quad (3)$$

where the last step is obtained by a direct multiplication. We define a $N \times N$ matrix \tilde{G}_x , with $(\tilde{G}_x)_{ij} = \alpha_i \langle c_i^\dagger c_j \rangle$, ($i, j = 1, 2, \dots, N$). A second key observation [28] is that different orders of principal minors for $\det \tilde{G}_x$ coincides with different order of terms for $\langle \hat{U}_x \rangle$

in Eq. (4) with Wick's theorem. As an example, we can see that the second order of principal minors of $\det \tilde{G}_x$

are $\alpha_i \alpha_j \begin{vmatrix} \langle \hat{n}_i \rangle & \langle c_i^\dagger c_j \rangle \\ \langle c_j^\dagger c_i \rangle & \langle \hat{n}_j \rangle \end{vmatrix}$, with $1 \leq i < j \leq N$, which

coincide with $\sum_{1 \leq i < j \leq N} \alpha_i \alpha_j \langle \hat{n}_i \hat{n}_j \rangle$ in Eq. (4) by using Wick's theorem to the latter form. Furthermore, assuming eigenvalues for \tilde{G}_x are λ_i ($i = 1, 2, \dots, N$), we have an identity for $\langle \hat{U}_x \rangle$ with eigenvalues as [29],

$$\langle \hat{U}_x \rangle = 1 + \sum_{l=1}^N \lambda_l + \sum_{1 \leq i < j \leq N} \lambda_i \lambda_j + \dots. \quad (5)$$

Compared with the characteristic polynomials $\det(\tilde{G}_x - \lambda I) = (-\lambda)^N + (-\lambda)^{N-1} \sum_{i=1}^N \lambda_i + (-\lambda)^{N-2} \sum_{1 \leq i < j \leq N} \lambda_i \lambda_j + \dots$, and setting $\lambda = -1$, we find

$$\langle \hat{U}_x \rangle = \det(\tilde{G}_x + I). \quad (6)$$

Therefore, finally we have the polarization in the formalism of Green's functions,

$$P_x = \frac{1}{2\pi\mathcal{S}} \text{Im} \left[\text{Tr} \ln \left(\tilde{G}_x + I \right) \right] - P_{bg}. \quad (7)$$

With the identity $\text{Tr} \ln A = \ln \det A$, we have obtained Eq. (1). We have a remark here for the numerical implementation. As is known that polarization is an intensive quantity. In practical calculations, one cannot adopt Eq. (7), of which the first term tends to go to zero in the thermodynamic limit in the more than one-dimensional space [30], because numerically the imaginary part of the logarithm function lies in the interval $[-\pi, \pi)$.

Similarly, we can write down the formula for the quadrupole moment in a crystal,

$$Q_{xy} = \frac{1}{2\pi\mathcal{L}} \text{Im} \left[\text{Tr} \ln \left(\tilde{G}_{xy} + I \right) \right] - Q_{bg}. \quad (8)$$

Here $\tilde{G}_{xy} = \alpha_{xy} G$, and $\alpha_{xy} = \text{diag}\{e^{\frac{2\pi i x_1 y_1}{L_x L_y}} - 1, \dots, e^{\frac{2\pi i x_N y_N}{L_x L_y}} - 1\}$. $\mathcal{L} = 1, L_z$ for two- and three-dimensional case, which is the length perpendicular to the $x - y$ plane. $Q_{bg} = \frac{n_f}{\mathcal{L}} \sum_i \frac{x_i y_i}{L_x L_y}$. A generalization to the case of the octupole moment is straightforward.

The key issue in the calculations in Eqs. (1) and (8) is to obtain the matrix of Green's function G , and we are interested in correlated systems described by the fermionic Hubbard model. It is necessary to obtain G of a correlated lattice model for calculating of many-body multipole moments. Real-space dynamical mean-field theory (R-DMFT) [20, 23–25] is perfectly suitable for this purpose. In this scheme, a strongly correlated system on a lattice is mapped into a group of impurities on lattice sites with the same spatial symmetry, along with hopping between different sites. In this way both the onsite interactions and the inhomogeneous due to hopping are

taken into account. One then solves the DMFT problem on all the sites until it is fully converged. Therefore, the interaction effects are taken into account on the DMFT level. Once the R-DMFT loop is converged, we then adopt Eqs. (1) and (8) to compute multipole indices. The flow chart for the whole computation process is shown in Fig. 1, which can be mostly divided into two parts: (1) the R-DMFT part, and (2) the computation of many-body multipole indices. We comment on the efficiency of this algorithm. The most time-consuming part would be the R-DMFT routines, which can be accelerated with parallel implementation and optimized by the spatial symmetry consideration. With convergent Green's function, the calculations of multipole indices are quite efficient.

To sum up, we have achieved two significant advancements. (1) We have a formula in the formalism of real-space Green's functions for the multipole indices, which is ready to be combined with the DMFT method, and one can further introduce disorders to lattices to explore the rich physics of disorder effects, quasi-crystal lattice [31], amorphous lattices [32, 33] and so on. (2) With the multipole indices as a bridge, one can certainly study the localization length of the electron [10], the polarization fluctuation [26], and the quantum geometric tensor [27] in the correlated lattices.

III. DEMONSTRATING R-DMFT CALCULATIONS OF THE INTERACTING BBH MODEL WITH STAGGERED POTENTIALS

In this section, we implement the multipole moment of the correlated BBH model based on Eqs. (1) and (8) with the real-space Green's function calculated by the R-DMFT, and discuss the correlation effects explicitly.

A. The interacting BBH Model

The interacting BBH model [12, 18] on a two-dimensional lattice with the Hubbard interaction and staggered potentials reads,

$$H = H_0 + H_{stagger} + U \sum_{\mathbf{R}\gamma} n_{\mathbf{R}\gamma\uparrow} n_{\mathbf{R}\gamma\downarrow},$$

where

$$\begin{aligned} H_0 = & \sum_{\mathbf{R}\sigma} \left[\gamma_x \left(c_{\mathbf{R}1\sigma}^\dagger c_{\mathbf{R}3\sigma} + c_{\mathbf{R}2\sigma}^\dagger c_{\mathbf{R}4\sigma} \right) \right. \\ & + \gamma_y \left(c_{\mathbf{R}1\sigma}^\dagger c_{\mathbf{R}4\sigma} - c_{\mathbf{R}2\sigma}^\dagger c_{\mathbf{R}3\sigma} \right) \\ & + \lambda_x \left(c_{\mathbf{R}1\sigma}^\dagger c_{\mathbf{R}+\hat{x}3\sigma} + c_{\mathbf{R}4\sigma}^\dagger c_{\mathbf{R}+\hat{x}2\sigma} \right) \\ & \left. + \lambda_y \left(c_{\mathbf{R}1\sigma}^\dagger c_{\mathbf{R}+\hat{y}4\sigma} - c_{\mathbf{R}3\sigma}^\dagger c_{\mathbf{R}+\hat{y}2\sigma} \right) \right] + H.c., \end{aligned}$$

and $H_{stagger}$ is the onsite staggered potential. The non-interacting part H_0 is a standard toy model of the higher-order topological insulator. In general, spatial symmetries are closely related to the quantization of the polarization and quadrupole moments [12, 18]. By the term $H_{stagger}$ we can tune the spatial symmetry, and explore the correlating effects by introducing the Hubbard interaction term. We are mainly interested in two cases with different spatial symmetries as follows: case (i) $H_{stagger} = \Delta_{xy} \sum_{\mathbf{R}\sigma} (n_{\mathbf{R}1\sigma} + n_{\mathbf{R}2\sigma} - n_{\mathbf{R}3\sigma} - n_{\mathbf{R}4\sigma})$ preserving the spatial inversion symmetry, and case (ii) $H_{stagger} = \Delta_x \sum_{\mathbf{R}\sigma} (n_{\mathbf{R}1\sigma} - n_{\mathbf{R}2\sigma} - n_{\mathbf{R}3\sigma} + n_{\mathbf{R}4\sigma})$ or $H_{stagger} = \Delta_y \sum_{\mathbf{R}\sigma} (n_{\mathbf{R}1\sigma} - n_{\mathbf{R}2\sigma} + n_{\mathbf{R}3\sigma} - n_{\mathbf{R}4\sigma})$ which respects mirror symmetry along the y -direction (or the x -direction).

B. Results and discussion

As a demonstration for our general protocol to calculate the multipole indices in correlated insulators, we present results for the polarization and quadrupole moments of the interacting BBH model when the onsite staggered potential is nonzero, which affords us a way to tune the spatial symmetry. For the R-DMFT part calculations, an impurity solver of iterative perturbation theory [20] is adopted. We choose the periodical boundary conditions for lattices, work at the half-filling with $n_f = \frac{1}{2}$, and focus on the paramagnetic phase. As a side remark, we point out that all the multipole moments data are presented by modulo 1.

1. Case (i)

As shown in Fig. 2, there are quantized polarization component P_x and sharp topological phase transitions in non-interacting case, which are features of the BBH model, and remarkably similar phenomena in interacting regimes. The results given by the formula (1) are consistent with the spatial symmetry analysis. In Fig. 2, we do not present results for P_y , whose features are quite similar to these for P_x . The onsite staggered potential Δ_{xy} breaks the reflection symmetries about both x and y axes, but keeps the inversion symmetry, which leaves the polarization quantized in Fig. 2 for non-interacting case (a), weakly interacting case (b) and strongly interacting case (c). Within the R-DMFT method, even though the interaction is turned on, the polarization component P_x keep quantized as long as the spatial symmetry conditions for quantization are preserved. In Fig. 2, we show the spectral functions for four different sites in one unit cell, and the gaps due to interactions together with emergent side-bands in Figs. 2(e-f) for very strong interactions clearly show that the system is driven into the Mott insulator phase when the interaction U is large enough. To sum up, we show that even in the correlating regime, the quantization of polarization is still determined by the

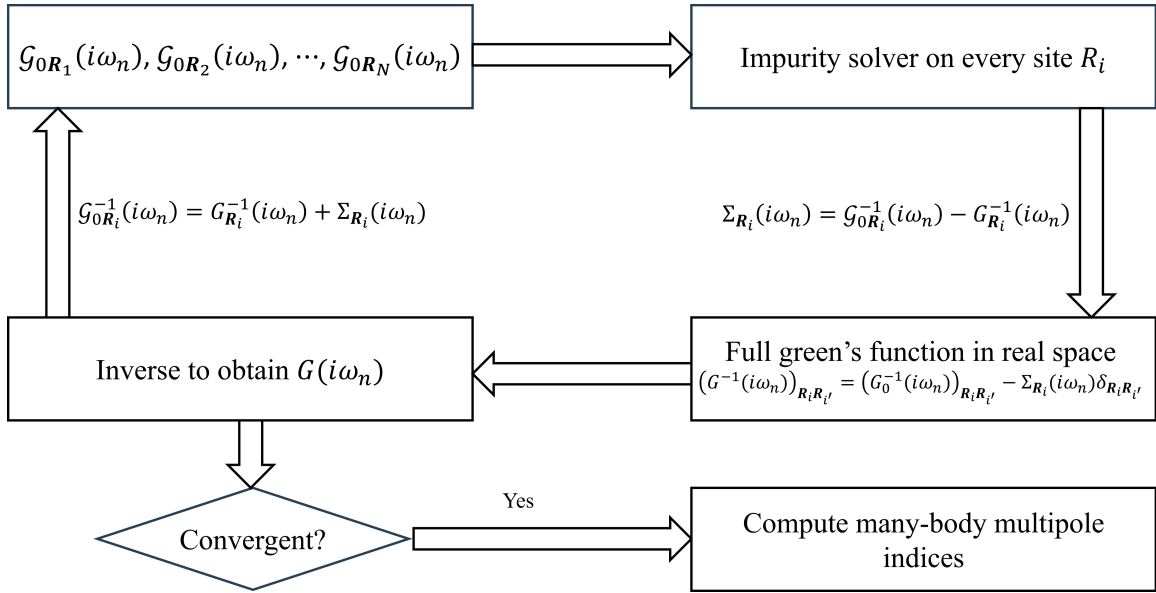


Figure 1. Flowchart to compute the many-body multipole indices with the real-space dynamical mean-field theory (R-DMFT) and the Green’s function formula for the multipole indices in the real-space. The R-DMFT is featured in Anderson impurities on every lattice site, self-consistently dealt with impurity solver to obtain $\Sigma_{\mathbf{R}_i}(i\omega_n)$ on site \mathbf{R}_i , and meanwhile, the hopping taken into account by $(G_0^{-1}(i\omega_n))_{\mathbf{R}_i \mathbf{R}_{i'}}$. The computation of the multipole indices takes place when the R-DMFT loop is convergent with the Weiss field $\mathcal{G}_{0\mathbf{R}_i}(i\omega_n)$.

spatial symmetries.

Furthermore, we present our results for the quadrupole moment calculations with Eq. (8) in Fig. 3. If the reflection symmetries are absent, the quadrupole moment Q_{xy} is unquantized in Figs. 3(a) with nonzero Δ_{xy} , and (c) with both Δ_{xy} and interaction U turned on. As long as the reflection symmetry is preserved in both x and y directions, the quadrupole moment stays quantized as shown in Fig. 3(b). It shows that the spatial symmetry is a dominant factor for the quantization of the quadrupole moment in the paramagnetic phase.

2. Case (ii)

In this subsection, we present our results for the polarization P_x and P_y for case (ii) with $H_{stagger} = \Delta_y \sum_{\mathbf{R}\sigma} (n_{\mathbf{R}1\sigma} - n_{\mathbf{R}2\sigma} + n_{\mathbf{R}3\sigma} - n_{\mathbf{R}4\sigma})$, which respects the mirror symmetry in the x direction. In Fig. 4(a) for non-interacting case with different strengths of Δ_y , (b) for weak interactions with finite Δ_y and (c) for strong interaction with finite Δ_y , we observe perfect quantization of the polarization P_x and clear topological transition when both the interaction and Δ_y is finite. Due to the spatial symmetry of case (ii), the topological transition here is in fact quite similar to that in the one-dimensional Su-Schrieffer-Heeger model [35]. As a sharp contrast in Figs. 4(d-f), we can see the quantization of P_y is broken once Δ_y is nonzero, indicating the broken of the mirror symmetry. By the comparison between P_x and P_y , we clearly see that the spatial symmetry is a vital factor for

the quantization of the polarization in the paramagnetic phase. As a side comment, in Figs. 4(a, d), we introduce a tiny $\Delta_x = 1 \times 10^{-6}$ to break the mirror symmetry with the x axis a little, as a numerical trick to remove the “degeneracy” between -0.5 and 0.5 for the polarization in the sense of modulo [18].

We have a few words on the experimental measurement. The prediction of the multipole moments is ready to be checked by experiment measurements. Even though it is difficult to realize the BBH model in real materials, it seems promising to do it in metamaterials [36, 37].

IV. SUMMARY AND OUTLOOK

To sum up, we propose a practical calculation scheme for the multipole moments in correlated materials on the level of R-DMFT. By calculations of BBH with different spatial symmetries due to staggered potentials, and different strengths of interactions we show the effectiveness of our method in exploring the properties of the multipole indices. However, its full potential is not fully unleashed. Our general method is ready to be implemented to explore a disordered correlated lattice. The close relation of polarization with the localization length [10], and the quantum geometric tensor [27] affords us a way to explore these interesting physical quantities. Our demonstrating calculations show that the spatial symmetry is a dominant factor for the quantization of the polarization and quadrupole moments even in the correlating regime, at least in the paramagnetic phase.

ACKNOWLEDGMENTS

T.Q. and J.H.Z. were supported by the National Natural Science Foundation of China under Grants No.12174394 and U2032164. J.H.Z. was also supported

by HFIPS Director's Fund (Grants No. YZJJQY202304 and No. BJPY2023B05) and Anhui Provincial Major S&T Project (s202305a12020005), the High Magnetic Field Laboratory of Anhui Province under Contract No. AHHM-FX-2020-02. A portion of this work was supported by Chinese Academy of Sciences under contract No. JZHKYPT-2021-08.

-
- [1] R. Resta, *Ferroelectrics* **136**, 51 (1992).
- [2] R. D. King-Smith and D. Vanderbilt, *Phys. Rev. B* **47**, 1651 (1993).
- [3] R. Resta, *Rev. Mod. Phys.* **66**, 899 (1994).
- [4] G. Ortiz and R. M. Martin, *Phys. Rev. B* **49**, 14202 (1994).
- [5] S. Coh and D. Vanderbilt, *Phys. Rev. Lett.* **102**, 107603 (2009).
- [6] D. Xiao, M.-C. Chang, and Q. Niu, *Rev. Mod. Phys.* **82**, 1959 (2010).
- [7] S. Vaidya, M. C. Rechtsman, and W. A. Benalcazar, *Phys. Rev. Lett.* **132**, 116602 (2024).
- [8] G. Ortiz, P. Ordejón, R. M. Martin, and G. Chiappe, *Phys. Rev. B* **54**, 13515 (1996).
- [9] R. Resta, *Phys. Rev. Lett.* **80**, 1800 (1998).
- [10] R. Resta and S. Sorella, *Phys. Rev. Lett.* **82**, 370 (1999).
- [11] W. Kohn, *Phys. Rev.* **133**, A171 (1964).
- [12] W. A. Benalcazar, B. A. Bernevig, and T. L. Hughes, *Science* **357**, 61 (2017).
- [13] B. Xie, H.-X. Wang, X. Zhang, P. Zhan, J.-H. Jiang, M. Lu, and Y. Chen, *Nat Rev Phys* **3**, 520 (2021).
- [14] Y.-B. Yang, J.-H. Wang, K. Li, and Y. Xu, *J. Phys.: Condens. Matter* **36**, 283002 (2024).
- [15] B. Kang, K. Shiozaki, and G. Y. Cho, *Phys. Rev. B* **100**, 245134 (2019).
- [16] S. Ono, L. Trifunovic, and H. Watanabe, *Phys. Rev. B* **100**, 245133 (2019).
- [17] W. Lee, G. Y. Cho, and B. Kang, *Phys. Rev. B* **105**, 155143 (2022).
- [18] W. A. Benalcazar, B. A. Bernevig, and T. L. Hughes, *Phys. Rev. B* **96**, 245115 (2017).
- [19] R. Nourafkan and G. Kotliar, *Phys. Rev. B* **88**, 155121 (2013).
- [20] A. Georges, G. Kotliar, W. Krauth, and M. J. Rozenberg, *Rev. Mod. Phys.* **68**, 13 (1996).
- [21] C. Peng, R.-Q. He, and Z.-Y. Lu, *Phys. Rev. B* **102**, 045110 (2020), publisher: American Physical Society.
- [22] B. Kang, W. Lee, and G. Y. Cho, *Phys. Rev. Lett.* **126**, 016402 (2021).
- [23] M. Potthoff, *Eur. Phys. J. B* **32**, 429 (2003).
- [24] R. Helmes, *Dynamical Mean Field Theory of inhomogeneous correlated systems*, PhD Thesis, Koln University (2008).
- [25] W. Hofstetter and T. Qin, *Journal of Physics B: Atomic, Molecular and Optical Physics* **51**, 082001 (2018).
- [26] R. Resta, *Phys. Rev. Lett.* **96**, 137601 (2006).
- [27] I. Souza, T. Wilkens, and R. M. Martin, *Phys. Rev. B* **62**, 1666 (2000).
- [28] S.-A. Cheong and C. L. Henley, *Phys. Rev. B* **69**, 075111 (2004).
- [29] C. D. Meyer, *Matrix Analysis and Applied Linear Algebra, Second Edition* (Society for Industrial and Applied Mathematics, Philadelphia, PA, 2023).
- [30] R. Resta, *J. Chem. Phys.* **154**, 050901 (2021).
- [31] D.-T. Tran, A. Dauphin, N. Goldman, and P. Gaspard, *Phys. Rev. B* **91**, 085125 (2015).
- [32] A. Agarwala and V. B. Shenoy, *Phys. Rev. Lett.* **118**, 236402 (2017), publisher: American Physical Society.
- [33] Y.-B. Yang, T. Qin, D.-L. Deng, L.-M. Duan, and Y. Xu, *Phys. Rev. Lett.* **123**, 076401 (2019).
- [34] H. J. Vidberg and J. W. Serene, *Journal of Low Temperature Physics* **29**, 179 (1977).
- [35] W. P. Su, J. R. Schrieffer, and A. J. Heeger, *Phys. Rev. B* **22**, 2099 (1980).
- [36] K. Yatsugi, T. Yoshida, T. Mizoguchi, Y. Kuno, H. Iizuka, Y. Tadokoro, and Y. Hatsugai, *Commun Phys* **5**, 180 (2022).
- [37] J. Dong, V. Juričić, and B. Roy, *Phys. Rev. Res.* **3**, 023056 (2021), publisher: American Physical Society.

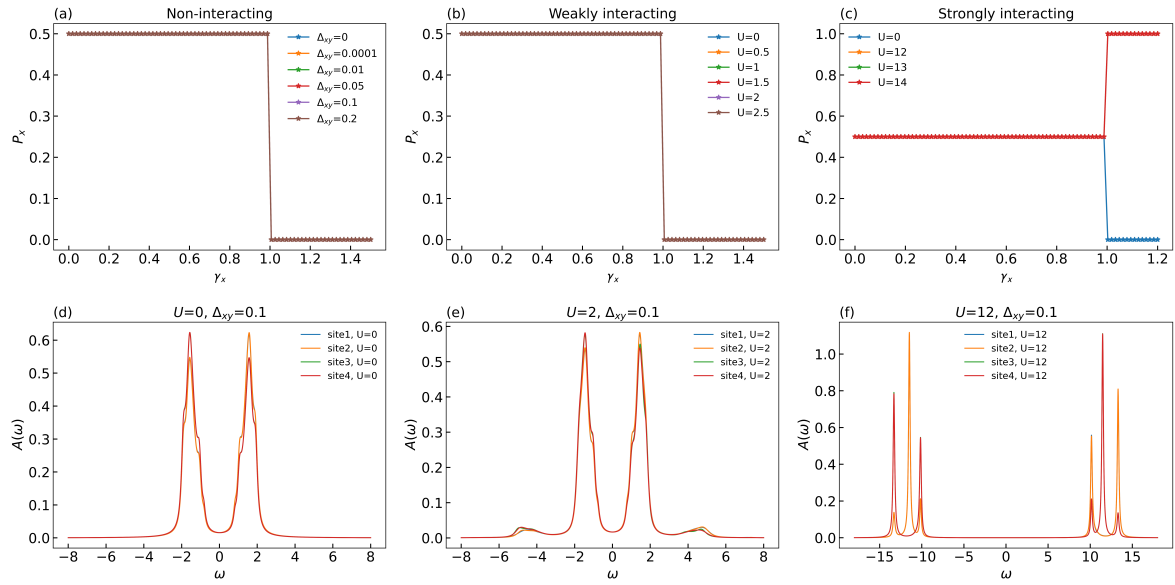


Figure 2. Case (i): (a-c) The polarization component P_x versus $\gamma_x(\gamma_y)$ of the BBH model for case (i) versus the staggered potential Δ_{xy} and the interaction strength U , with a lattice size of 12×12 and $\gamma_y = \gamma_x$, and (d-f) spectral functions for different interactions with $\gamma_x = \gamma_y = 0.4$. We have $\lambda_x = \lambda_y = 1$ as the energy unit. In panel (a) we explore different Δ_{xy} when $U = 0$. And with a fixed $\Delta_{xy} = 0.1$ we present P_x for weak interaction in panel (b) and strong interaction in panel (c). For the DMFT calculations, $\beta = 50$, the number of Matsubara frequencies is 256, and the Pade approximation [34] is adopted in the analytical continuation of Green's function to the real frequency.

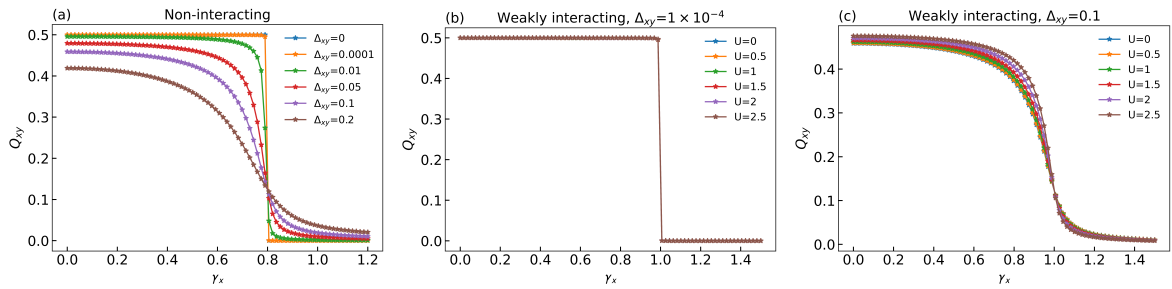


Figure 3. Case (i): The quadrupole moment Q_{xy} versus $\gamma_x(\gamma_y)$ of the BBH model with a lattice size of 12×12 for (a) noninteracting case with different strengths of Δ_{xy} , (b) interacting case with $\Delta_{xy} = 1 \times 10^{-4}$, and (c) interacting case with $\Delta_{xy} = 0.1$. $\gamma_x = \gamma_y$. Other parameters are the same as these in Fig. 2.

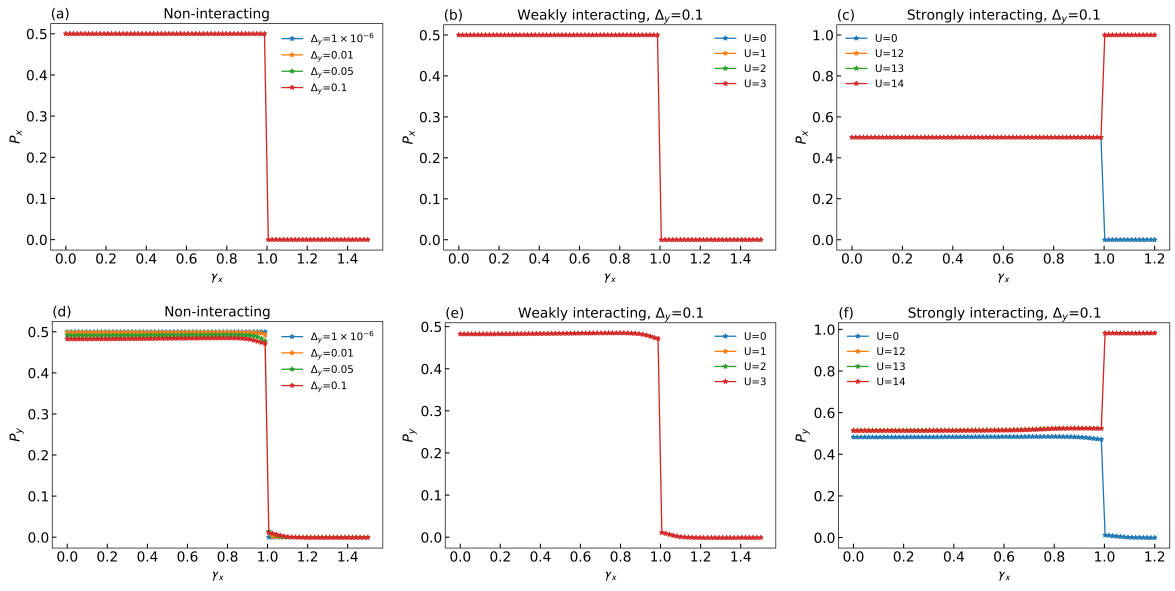


Figure 4. Case (ii): The polarization components P_x and P_y versus $\gamma_x(\gamma_y)$ of the BBH model with a lattice size of 12×12 . We present results for P_x and P_y , in (a, d) for non-interacting case with different strengths of Δ_y , (b, e) for weak interactions with finite Δ_y and (c, f) for strong interaction with finite Δ_y . $\gamma_x = \gamma_y$. Other parameters are the same as these in Fig. 2.